Dynamic Mechanical Signatures of a Polyester-Urethane and Plastic-Bonded Explosives Based on this Polymer†

D. MARK HOFFMAN

Energetic Materials Center, Lawrence Livermore National Laboratory, Livermore, California 94550

Received 22 January 2001; accepted 24 February 2001

ABSTRACT: The complex shear moduli of the segmented polyurethane Estane 5703p, Livermore explosive (LX)-14, and plastic bonded explosive (PBX)-9501, which use this polymer as a binder, have been investigated. Segmented polyurethanes, such as Estane 5703, contain microphase-separated hard segments in a rubbery matrix of soft segments. LX-14 is composed of 95.5% 1,3,5,7-tetranitroazacyclooctane (HMX) explosive with 4.5% Estane 5703 binder. PBX-9501 is composed of 94.9% HMX, 2.5% Estane 5703p binder, 2.5% nitroplasticizer (NP), and about 0.1% antioxidant Irganox 1010. In the temperature range from −150 to 120°C, two relaxations were observed as peaks in the loss modulus and tangent delta in Estane 5703p and LX-14. A third relaxation was found in PBX-9501. The low temperature relaxation associated with vitrification of the poly(ester urethane) soft segment occurred in the shear loss modulus (G'') at −29 and −26°C in Estane and LX-14, respectively, at 1 Hz. In PBX-9501 the Estane soft segment glass transition peak, T_g(SS), in the loss modulus occurred at −40 ± 3°C at 1 Hz. The reduction in soft segment glass transition in PBX-9501 is clear evidence of plasticization of the soft segment by NP. The apparent activation energy of the maximum in the loss modulus for LX-14 and PBX-9501 over the frequency range from 0.1 to 10 Hz was 230 kJ/mole (55 kcal/mole). The hard segment glass transition, T_g(HS), was observed as a peak in the loss modulus at about 70°C. In LX-14 the transition was observed at lower temperatures (56–58°C at 1 Hz) depending on thermal history. There was a low temperature shoulder on the T_g(HS) of Estane 5703 associated with soft segment crystallinity. Modulated differential scanning calorimetry (MDSC) was used to verify the T_g(HS) in Estane and 50/50 mixtures of Estane with NP. In PBX-9501 the hard segment glass transition occurred between 65 and 72°C. The presence of NP in PBX-9501 gave rise to a new transition, T_{eu}(NP), between 8 and 15°C. This peak is believed to be associated with the eutectic melting of the plasticizer. Returns of fielded PBX-9501 that were 6 and 11 years old were also measured. Small variations in T_g(SS) and the rubber plateau modulus were observed in these aged samples, consistent with migration of plasticizer and/or very low levels of chain scission. © 2002 John Wiley & Sons, Inc.* J Appl Polym Sci 83: 1009–1024, 2002

Key words: plastic-bonded explosives; polyurethane binder; dynamic mechanical analysis; differential scanning calorimetry; coefficient of expansion

INTRODUCTION

The segmented poly(ester urethane) Estane 5703p manufactured by BF Goodrich is used by Lawrence Livermore National Laboratory (LLNL) and Los Alamos National Laboratory (LANL) to formulate 1,3,5,7-tetranitroazacyclooctane (HMX)-based explosives LX-14 and PBX-9501, respectively. LX-14 is a 95.5/4.5 wt % composite of HMX/Estane 5703p used in high performance shaped charges such as Hell Fire and TOE 2. It contains no plasticizer. PBX-9501 is similar except that the Estane polyurethane has been plasticized with the eutectic mixture of

Correspondence to: D. Mark Hoffman (hoffman2@llnl.gov).
Contract grant sponsor: Work performed under the US Department of Energy under contract W-7405-Eng-48.

Journal of Applied Polymer Science, Vol. 83, 1009–1024 (2002)

DOI 10.1002/app.2281

bis(2,2′-dinitropropyl)formal and bis(2,2′-dinitropropyl)acetal commonly referred to as nitroplasticizer (NP). PBX-9501 is a 95/2.5/2.5 wt % composite of HMX/Estane 5703p/NP used in LANL-designed weapons.

Estane 5703p is composed of the reaction product of 4,4′-methylene bis(phenylisocyanate) (MDI) and butanediol (BDO) hard segments in a matrix of poly(butylene adipate) soft segments.[1] The hard and soft segment glass transitions of this binder occur at −28 and 80°C, respectively.[1–4] Plasticization with 50% NP reduces the glass transitions to −45 and 72°C, respectively. The butylene adipate soft segment is susceptible to ester hydrolysis[5–11] and the effect of chain scission on the modulus and strength of the PBX appears to depend on the binder weight average molecular weight.[9]

Three classes (particle size distributions) of HMX are used in LX-14 and two classes in PBX-9501.[12,13] Class 1 HMX has an average particle size of approximately 150–250 μm. Class 2 HMX is relatively fine with a mean particle size of 2–4 μm. LX-14 also contains LX-04 grade HMX that consists of a bimodal mixture of 25/75 ratio of 12- and 120-μm particles. These plastic-bonded explosives are prepared by precipitation of a water-saturated solution of Estane 5703p in methylethyl ketone (MEK) onto an HMX/water slurry in a Holston reactor.[14] When the solvent is removed, the resulting "molding powder" consists of spherical aggregates of HMX explosive crystals coated with polymer.[15] This "molding powder" is dried, isostatically pressed into billets at 105°C and 140 MPa (20 Ksi) for LX-14 and somewhat lower temperature for PBX-9501, cooled to ambient and machined into device parts. LX-14 can also be pressed to near-net shape for military applications.

Although the static mechanical properties of LX-14 and PBX-9501 are known,[12,16] these results were only measured at a few temperatures and rates. Dynamic mechanical data on a few explosives and propellants have been published,[17–20] but no systematic study of LX-14 or PBX-9501 has been done. This report is an attempt to generate baseline and field aged dynamic mechanical properties of these explosives.

EXPERIMENTAL

LX-14 and PBX-9501 Explosive Samples

Specimens of LX-14 were prepared from lot C-212 manufactured at Holston Army Ammunition plant, HAAP, in 1996, and stored at Lawrence Livermore Labs in the explosive bunkers prior to pressing and machining. There was no further preparation or treatment of these samples prior to measurement. Three sets of samples of PBX-9501 were obtained from Los Alamos National Laboratory: one set (C) of control samples from old, unfielded molding powder, a second set (E) of 5.75-year-old field returned samples, and a third set (D) of 11-year-old field returned samples. A final set of PBX-9501 samples was prepared from new Estane 5703p, with old NP and HMX. Table I lists the explosives used in the dynamic mechanical experiments.

Dynamic Mechanical Measurements

Complex shear moduli were measured on a Rheometrics Mechanical Spectrometer (RMS) model 800. Rectangular specimens 6.35 cm (2.5″) long by 1.27 cm (0.5″) wide by 0.3175 cm (0.125″) thick were machined to approximately 0.003 cm tolerances. The RMS 800 has special fixturing to hold these samples inside a thermal chamber cooled by gas generated from liquid nitrogen and heated by an electronic heating element. Five frequencies were measured at a given temperature. Temperature was controlled to approximately ±0.3°C during the frequency sampling. Temperature was incremented in 3 or 5°C steps and allowed to

Table I Sample Histories of LX-14 and PBX-9501 Used in These Experiments

Sample ID	Lot No.	History/Remarks
LX-14A	C-212	Manufactured at HAAP in 1996
PBX-9501C	730-010	Control sample from old stored PBX-9501 molding powder
PBX-9501PR	PR1185	Prepared in house from new Estane 5703 and old NP, HMX
PBX-9501E	730-004	Taken from fielded explosive after 5.75 years
PBX-9501D	730-003	Taken from fielded explosive after 11 years

equilibrate for one minute prior to resumption of modulus measurements. After each temperature step, the specimen height was electronically adjusted to maintain a slight compressive load to compensate for thermal expansion and prevent buckling. The maximum percent strain was set to 0.1%. Frequency was varied from 0.1 to 10 Hz in 5 logarithmic increments during each temperature interval. All explosives testing was performed remotely in a $\frac{3}{4}''$ steel cell. For the rectangular torsional specimen geometry, a sinusoidal strain, γ^* is imposed on the specimen according to the relationship

$$\gamma^* = \gamma_0 \exp[i(\omega t)] \tag{1}$$

where γ_0 is the maximum strain amplitude, ω is the oscillating frequency, and t is the time. The shear stress τ^* is measured as a torque that lags behind the imposed strain by some time δ/ω according to the relationship

$$\tau^* = \tau_0 \exp[i(\omega t + \delta)] \tag{2}$$

where δ is the phase angle of this lag. In the linear viscoelastic regime, the modulus is independent of strain so the complex shear modulus is given by

$$G^* = (\tau^*/\gamma^*) = (\tau_0/\gamma_0)e^{i(\delta)} = G' + iG'' \tag{3}$$

where G' is the shear storage modulus (real component of G^*) and G'' is the shear loss modulus (imaginary component of G^*). The ratio of G''/G' is the tangent of the loss angle δ. When a relaxation occurs in a material, there is a time- or frequency-dependent effect on the modulus. This results in a reduction of the storage modulus and a maximum in the loss modulus and tangent δ. Various types of transitions show such relaxations including glass transitions, secondary relaxations, and crystallization or melting phenomena.

RESULTS AND DISCUSSION

Binder

Estane 5703 is a poly(ester urethane) composed of polybutylene adipate soft blocks connected by up to 7 repeating units of urethane linkages from the reaction product of methylene bis(diphenylisocyanate) and butanediol.[11] It is generally believed that microphase separation of these urethane hard segments is responsible for self-reinforcement in the polymer.[21–23] When segmented urethanes are cast from solvents with solubility parameters similar to the hard segment, soft gums are often formed. When they are cast from solvents with solubility parameters similar to the soft segment, more rubbery elastomers are formed. In processing PBX-9501, a water-saturated methylethylketone solution is used and the resulting 50% nitroplasticizer swollen Estane 5703 retains its shape like a crosslinked, swollen rubber at ambient, but can be processed with heat. Casting from pure MEK or acetone generates a much gummier material. This is generally interpreted as a varying degree of hard segment phase separation.

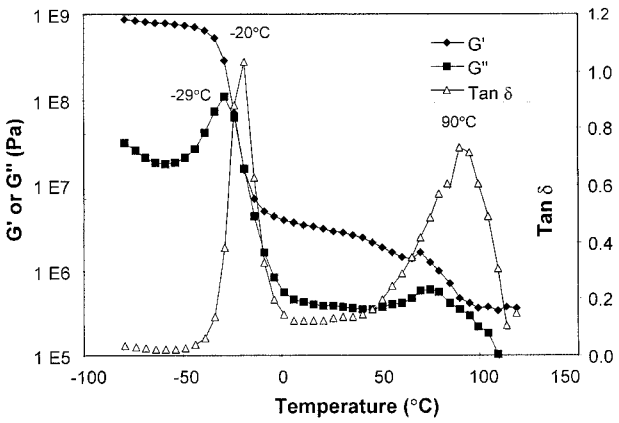

Figure 1 Dynamic mechanical measurements of Estane 5703p at 1 Hz showed 2 peaks in the loss modulus and tangent δ associated with the glass transition of the soft segment [$T_g(\mathrm{SS})_\delta = -20°\mathrm{C}$] and hard segment [$T_g(\mathrm{HS})_\delta = 90°\mathrm{C}$].

The Estane 5703p[1–4] binder in LX-14 and PBX-9501 has two relaxations in its dynamic mechanical spectrum that are expected to be observed in the explosives also. Figure 1 shows the dynamic mechanical spectrum of Estane 5703p measured at 1 Hz from −150 to 120°C. In the tangent δ the low temperature soft segment relaxation occurred at −18.9°C at 1 Hz. In the loss modulus the soft segment glass transition occurred at −29.1°C. The soft segment transition temperature was consistent with the Estane 5703 data of others (Flowers[3] = −29°C; Grotheer[1] = −27 to −28 for as received Estane, −24 to −26°C for precipitated).

In the tan δ trace the hard segment relaxation was observed as a peak at 90°C at 1 Hz. There is some evidence in the literature that soft segment

crystallization[21,24] may be responsible for the shoulder on the low temperature side of the tan δ peak. To help understand the hard segment relaxations, modulated differential scanning calorimetry (MDSC) was used. Two MDSC traces of Estane 5703p are shown in Figure 2. In the first run, a melting endotherm in the total heat flow trace started near 35°C, continued to perhaps as high as 100°C, and obscured the hard segment (HS) glass transition. The reversible component showed the hard segment glass transition in the first run at 80°C, slightly lower than the peak in tan δ. The glass transition of pure MDI-BDO polyurethane has been reported at 110°C.[25,26] There is considerable controversy about the presence or absence of a discontinuity in specific heat for MDI-BDO hard segments,[27,28] but this result was observed in two separate runs on pristine pellets of Estane. Recently similar MDSC results for a different hard segment have been reported.[29] In a second run, also shown in the figure, no T_g(HS) was found. This is consistent with mechanical and thermal measurements[30–32] where the hard segment in Estane 5703 develops over a period of several days after heating the polymer above its hard segment T_g. Note also that the soft segment T_g is not observed in the first run reversible MDSC trace, but is clearly evident in the total trace in both runs. The soft segment transition increased by 10–18°C in the second trace indicative of phase mixing with hard segments.[33–35] Reassociation of the hard segments can require several days.

MDSC was also used to identify the transitions in the 50/50 wt % NP/Estane 5703 binder system

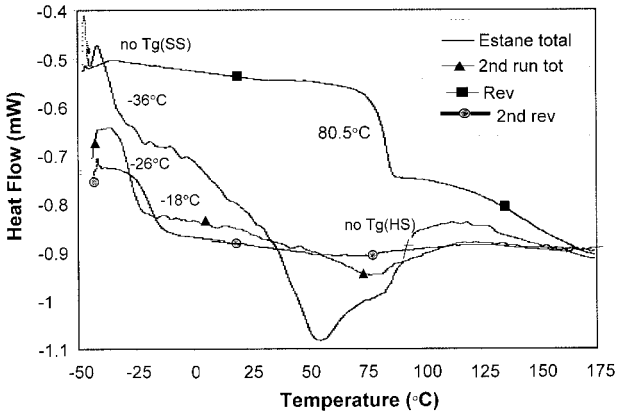

Figure 2 MDSC traces of Estane 5703p showed soft segment melting below the glass transition of the MDI/BDO hard segment at 80.5°C. Second run showed no T_g(HS).

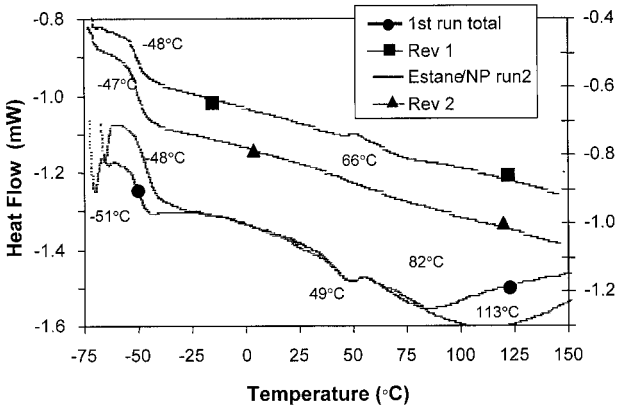

Figure 3 Estane/NP MDSC traces showed plasticization of both hard and soft segments. Second run again showed no T_g(HS).

used in PBX-9501. First and second MDSC traces of NP plasticized Estane 5703p prepared during the formulation and processing of PR-1185 samples of PBX-9501 are shown in Figure 3. At a heating rate of 3°C/min with a 1°C/min superimposed oscillation, the soft segment glass transition was observed at between −51 and −48°C for first and second runs. NP plasticization was not observed with GAP or PEG polyurethanes,[36] but is consistent with dynamic mechanical results on PBX-9501. The large variation in T_g(SS) between first and second MDSC traces was not observed in the 50/50 plasticized binder. The first-run T_g(SS) was only 4°C lower in the total heat flow trace and nearly identical in the reversible trace. The reason for this may be either that the hard segment is less effective at restricting soft segment mobility with 50% plasticizer present or that the hard segment phase separates more readily in plasticized soft segments. In the plasticized urethane, again an endotherm obscured the hard segment glass transition in the total heat flow trace. This endotherm was weaker, beginning at as low as 5°C, peaking at nearly the same temperature (45–56°C) and continuing up to 105–110°C. In first-run DSC traces, this endotherm contained a second peak at 82°C. In the second run, the first peak remained almost exactly at 49°C, and the second peak increased to 113°C. If this endotherm is associated with crystallization of the ester soft segment, the glassy hard segments have inhibited crystallization in the first run. The midpoint of the discontinuity in the first run reversible heat flow curve observed at 66°C was assumed to be the hard segment glass transition. In the second run, this weak discontinuity was not observed.

This again seems to imply some time is required for the hard segment to reassociate.

Plastic Bonded Explosives

The binder transitions in the dynamic mechanical spectrum of LX-14 and PBX-9501 were less dramatic since the explosives contain only 4.5 or 2.5% binder, respectively. Figure 4 shows the dynamic mechanical spectrum of LX-14 plastic-bonded explosive. The soft segment glass transition temperature of the Estane 5703p occurred at −26.1°C in the loss modulus and slightly higher (−21.3°C) in the tangent δ at 1 Hz. This glass transition temperature was slightly higher than that observed in the pure polymer. Grotheer[1] reprecipitated the binder from the solvent used in processing the explosive and found that the glass transition increased by 2°–3°. This is apparently due to removal of low molecular weight, unreacted oligomer during the PBXing process.

The hard segment glass transition in LX-14 was only observed in the loss modulus at between 58 and 70°C. The loss modulus peak was broad and shifted to higher temperatures on reheating as shown in the overlapping data in Figure 4. It is assumed that varying degree of perfection or incorporation of soft segment in the hard segment during the original vitrification process was annealed out at elevated temperature resulting in the observed increase in the loss modulus peak. Increased ordering of the hard segment is also consistent with the increase in storage modulus

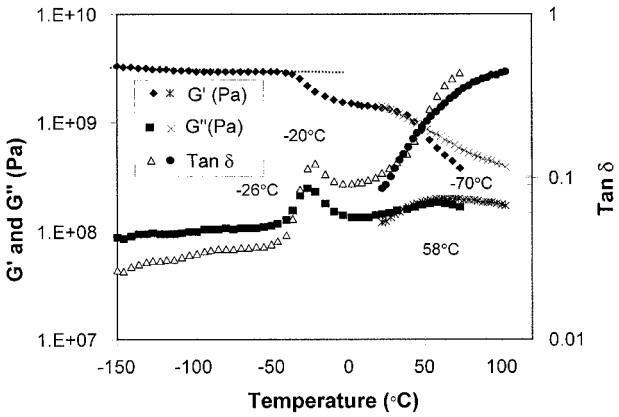

Figure 4 Dynamic mechanical response of LX-14 (Lot 211) at 1 Hz showed the Estane T_g(SS) as a maximum in the loss modulus at about −26°C and at slightly higher temperature in tan delta (−20°C). A second peak in the loss modulus occurred at 58°C, possibly associated with the hard segment glass transition.

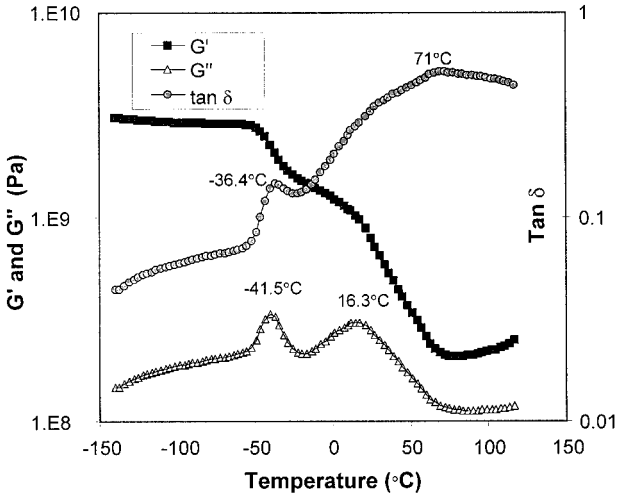

Figure 5 PBX-9501 control sample (C3_1) showed NP plasticization of Estane hard and soft segments and a transition associated with NP eutectic.

observed on the second heating. This maximum in the loss modulus peak in LX-14 was substantially less than that observed in the pure binder (74.9°C). No peak in tangent δ was observed in LX-14 below 120°C. Because of the possibility of thermal explosion, testing above 120°C was not performed.

The introduction of nitroplasticizer in PBX-9501 reduced the Estane 5703p soft segment glass transition by about 15°C. Figure 5 shows the dynamic mechanical spectra of a control sample of PBX-9501. The loss modulus peak at 1 Hz occurred at −41.5°C and the tangent δ peak was found at −36°C. Assuming a Fox[37] relationship,

$$1/T_g = \phi_1/T_{g1} + \phi_2/T_{g2} \tag{4}$$

where T_{g1} and T_{g2} are glass transitions, ϕ_1 and ϕ_2 are the weight fractions for the unplasticized soft segment and the NP, and T_g is the glass transition temperature of the plasticized soft segment. For plasticization of the Estane 5703 soft segment, the vitrification temperature of NP (T_{g2}) was approximately −51.4°C.

In PBX-9501 a new relaxation was observed between 6 and 18°C (see Fig. 5). NP has a eutectic temperature of 12°C,[38] but will readily supercool. This peak is probably associated with a change in mobility of NP in the PBX near its eutectic temperature (T_{eu}). If this transition were the Estane hard segment, assuming the Fox relation, with −51°C for T_g(NP) and equivalent solubility in both hard and soft segments, the hard segment

Table II DMA Soft Segment Transitions of Estane 5703 and Its PBXs[a]

Sample	Lot No.	$T_g(SS)_\delta$ (°C)	$T_g(SS)_G$ (°C)	$T_g(HS)_\delta$ (°C)	$T_g(HS)_G$ (°C)
Estane 5703p	8857	−18.9	−29.1	90	70
LX 14A	C-211	−21.3	−26.1	—	56
LX-14A′cool	C-211	−23.3	−26.2	NA	NA
LX-14A′	C-211	−18.4	−23.2	—	56
PBX-9501C	730-010	−37.0	−41.5	71.0	16.3
PBX-9501P	PR-11851	−36.5	−40		10
PBX-9501D	730-003	−36	−40	65, 75	5.6–13
PBX-9501E	730-004	−33.5	−41	65.4, 75.5	6.3–21

[a] Data taken at 1 Hz.

glass transition temperature would be approximately 85°C. This temperature is higher than 75 or 70°C observed in loss modulus measurements on pure Estane and LX-14, respectively. The stiffness of PBX-9501 above T_{eu} would also suggest it is not the hard segment T_g. The MDSC traces of the plasticized binder showed T_g(HS) at about 66°C and no major transitions in this temperature range. All these reasons lead us to believe that the plasticizer is responsible for this peak.

The tangent δ curve had a shoulder in this area (18–20°C) and a peak at 71.0°C. Although this peak is not clearly shown in the loss modulus, it is sufficiently close to the MDSC results to be associated with the hard segment glass transition. If this temperature is correct, applying the Fox equation yields only about 16–18% NP in the hard segment. This result is consistent with small angle X-ray data[39] showing selective incorporation of NP in the Estane soft segment. No evidence of MDI-BDO crystallization was observed in any of these experiments or in MDSC experiments up to 250°C. The melting temperature for MDI-BDO hard segments has been observed between 150 and 200°C depending on the hard segment content and perfection of the crystallites.[26,27,40] Overturf et al.[11] have shown that the average number of repeats of the MDI-BDO hard segment in Estane 5703 is 3–4 with some as high as 7. From the percentage C, H, N, and O in Estane 5703p,[1] the hard segment content could not exceed 30%. This is probably insufficient to form viable urethane crystals. Table II lists the dynamic mechanical transition temperatures observed at 1 Hz for pure binder and both explosives.

Subambient Behavior

The Soft Segment Glass Transition. As the temperature was increased from −150 to 0°C, Estane 5703 passed through its soft segment glass transition observed as a peak in the loss modulus and tangent δ at −29 and −19°C, respectively. In LX-14 the maximum associated with binder soft segment transition occurred at about −25 ± 2°C in G'', a slightly higher temperature than in the pure binder. In PBX-9501 NP plasticized the soft segment and the glass transition temperature is reduced by 13–15°C. Field aged samples of PBX-9501 were also measured. Tables II and III list the soft segment transitions observed in these samples.

The frequency dependence, $\omega(T)$, of the relaxation peak temperature in Estane 5703 and NP transitions may been modeled as an Arrhenius relationship:

$$\omega(T) = Ae^{-[E/RT(\text{peak})]} \tag{5}$$

Flowers[3] reported an activation energy of 250 kJ/mole (60 kcal/mole) for Estane 5703 and 280 kJ/mole (67 kcal/mole) for the PBX-9501 binder system, Estane/NP : 50/50. Figure 6 shows plots of the frequency dependence of peak temperatures for the soft segment transitions in LX-14 and PBX-9501. The activation energy of the G'' relaxation measured in this way for LX-14 and PBX-9501 were virtually identical at 230 ± 8 kJ/mole (55 ± 2 kcal/mole). The apparent activation energy for the tan δ relaxation was about the same but more scattered at 221 kJ/mole (53 ± 5 kcal/mole). These values were slightly lower than those of Flowers for the binder.

Table III Peak Temperatures in the Loss Modulus and tan δ at 1 Hz from Various Samples of PBX-9501

Sample ID	$T_g(SS)_{G''}$	$T_g(SS)_{\delta}$	$T_{eu}(G')$	$T_G(HS)_{\delta}$	Remarks and dT/dt
C2-1	−39.2	−34.9	6.6	Cool	SPME,[a] 1.05
C3-1	−41.0	−37.5	12.3	69.7	1.0°C/min
C3-2	−33.1	−29.5	14.0	63.1	2.33°C/min
PR1-1	−40.0	−35	10	Cool	−1.01°C/min
PR1-2	−40	−38	13.1	Break 40°C	1.05°C/min
PR2-1	−37.1	−34.0	—	Cool	−1.04°C/min
PR2-2	−33.9	−31.1	13.3	Break 60°C	1.17°C/min
D2-1	−41	−36	5.6	Cool	−1.66°C/min
D2-2	−40.9	−36.3	8.1	65.1[b]	1.46°C/min
D2-3	−36.1	−32.7	9.0	Break 50°C	1.46°C/min
D3-1	−40.1	37.2	13.0	75.0	1.49
E2-2	Frozen over		16.0	75.5	1.60°C/min
E2-3		−29.	8.0	Cool	−1.45°C/min
E2-4	−38.1	−31.1	4.4	63.0	1.41°C/min
E3-1	−42.2	37.4	6.0	71.8	1.45°C/min

[a] SPME: sample heated at 50°C for ~ 1 week prior to testing.
[b] Sample cracked during testing at approximately 65°C.

Time–Temperature Superposition. When long time or low frequency behavior is inconvenient to measure, in some instances modulus measurements can be made over short frequency spans at incremental temperatures and shifted about a reference temperature to cover a much larger time or frequency range.[41,42] For a wide variety of amorphous polymers, the WLF equation has been used for time–temperature superposition of the modulus about the glass transition temperature:

$$\log a(T) = -[C_1(T - T_r)]/[C_2 + T - T_r] \quad (6)$$

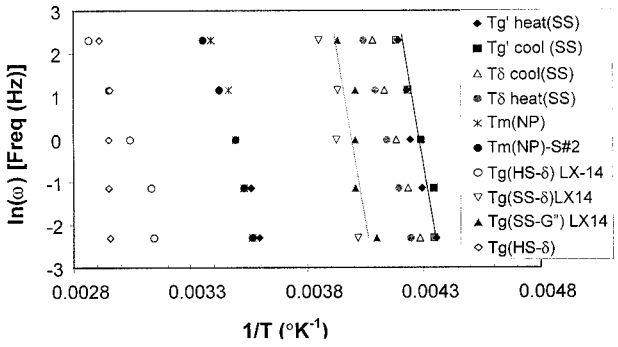

Figure 6 Arrhenius frequency dependence of the peaks in the soft segment glass transitions for LX-14 and PBX-9501 gave similar activation energies even though PB-9501 is heavily plasticized.

where $a(T)$ is the amount a modulus measurement made at frequency ω and temperature T must be shifted with respect to the reference temperature T_r (usually the glass transition) to produce a continuous modulus curve as a function of frequency. C_1 and C_2 are constants. The Rheometrics Orchestrator time–temperature superposition program was used to calculate the shift factor, $a(T)$, for a set of data over the temperature range from −65 to 25°C using different reference temperatures. This program allows the calculated shift factor to be fitted to either an Arrhenius or WLF relationship. Figure 7 shows typical shift factors generated by the program using linear optimization of shifts of G', G'', and torque data from LX-14 and PBX-9501. WLF fits were performed for several reference temperatures and T_r, C_1, and C_2, and the correlation coefficient for the best fit are given in Table IV. As can be seen in the figure, at lower temperatures the WLF equation over estimates the required shift factor. However, within the range investigated the fit was reasonable.

When the data for LX-14 were shifted, the T_r of −18.6°C produced the best correlation coefficient. At this temperature C_1 and C_2 were 5.9211 and 38.423, respectively. From the LX-14 shift factor in Figure 7, master curves for G', G'', and tan δ were generated about this reference temperature.

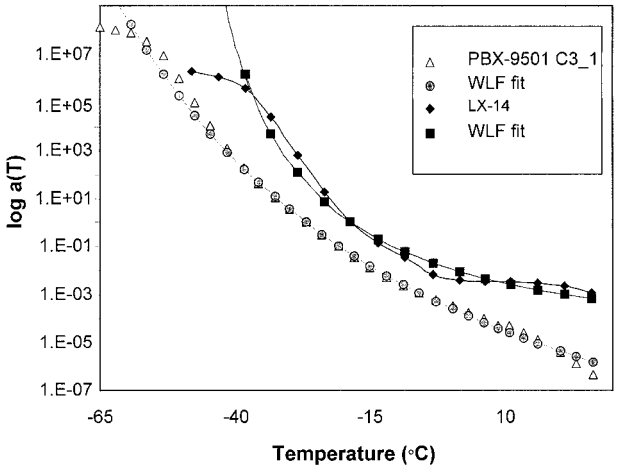

Figure 7 The time–temperature superpositon of G', G'', and torque for LX-14 and PBX-9501 measurements over the temperature range from −65 to 25°C compared well with WLF relationship except at low temperature.

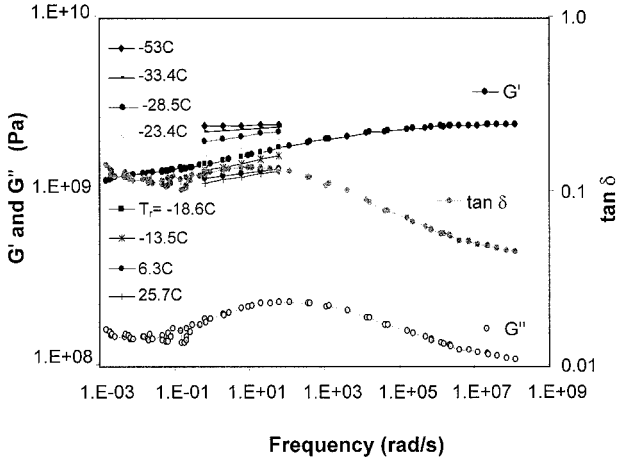

Figure 8 A master curve for LX-14 based on the shift factor in Figure 8 showed reasonable fits until ambient. Also shown are unshifted G' data at several temperatures.

The results span 12 orders of magnitude in frequency (see in Fig. 8). Some of the measured values for the shear storage moduli at various temperatures and 5 frequencies from 0.628 to 62.8 rad/s that were shifted to generate the master curve for G' are also shown at their measured frequencies in Figure 8. There was some scatter in the LX-14 loss modulus and tan δ master curves between 0.001 and 0.0001 rad/s, but for such a large range of frequencies and a composite explosive, the fit was quite reasonable.

Master curves were generated for PBX-9501 by optimizing G', G'', and torque shifts for different reference temperatures to obtain the best WLF correlation coefficient. When G', G'', and torque data were shifted about −30°C, the best WLF fit for sample C3_1, shown in Figure 7, gave C_1 of

Table IV Arrhenius Activation Energies and WLF Shift Factors for LX-14 and PBX-9501 Samples Shifted About the Estane 5703 Binder Glass Transition Temperature

Sample ID	Eact (G'') (kJ/mol)	Eact (δ) (kJ/mol)	T_r (°C)	C1	C2	Correlation
LX-14[a]	230 ± 8	220 ± 20	−18.6	5.9211	38.423	0.9010
PBX-9501[b]						
C3-1	237	246	−29.9[b]	16.869	94.459	0.9592
C3-2	226	—	−28.4	24.97	134.56	0.7940
PR1-1	213	191	−48.7	27.75	99.8	0.9098
PR1-2	233	189	−22.7	14.77	88.933	0.9784
PR2-1	187	225	−36.9	42.36	219.56	0.7058
PR2-2	237	221	−13.3	18.702	124.59	0.9321
D2-1	211	226	−9.16	26.255	190.0	0.8772
D2-2	252	184	1.23	53.069	373.27	0.571
D2-3	217	185	−22.6	19.052	115.21	0.9080
D3-1	223	280	−37.3	15.533	82.185	0.8627
E2-3	191	198	−38.7	26.71	129.86	0.9121
E2-4	190	169	−33.5	22.4	130.41	0.8075
E3-1	233	227	−37.5	19.101	92.688	0.8777

[a] Temperature range of fit = $-50 > T > 25$°C.
[b] Temperature range = $-65 > T > 25$°C.

16.869 and C_2 of 94.459. Again, the WLF fit predicts too large a shift below −60°C. Table IV lists the results of Arrhenius activation energies for fits to the peaks in G'' and tan δ and also WLF coefficients for best fits shifting over the temperature range from −65 to 25°C. A master curve for this sample of PBX-9501 using the shift factor in Figure 7 is shown in Figure 9. Some of the measured shear storage moduli and tangent δ data that were shifted are shown in a horizontal column between 0.628 and 62.8 rad/s in this figure also. Although the shift is quite good, some discrepancies are seen at the low frequency end (high temperature) of the master curves for G'' and tangent δ. This implies that the time–temperature superposition principle should be applied with caution in this region since other transitions may effect the results.[41,42]

The WLF coefficients can be calculated for any temperature once one set is known using

$$C_1(T) = C_1(T_r)^*C_2(T_r)/[C_2(T_r) + T - T_r] \quad (7)$$

and

$$C_2(T) = C_2(T_r) + T - T_r \quad (8)$$

When the coefficients for all the PBX-9501 samples with correlation coefficients of 0.7 or better were calculated using $T_g = T_r = -40$°C, the average C_1 was 22.7 ± 4.6 and the average C_2 value was 104 ± 27. These are not especially close to the universal values proposed by Ferry.

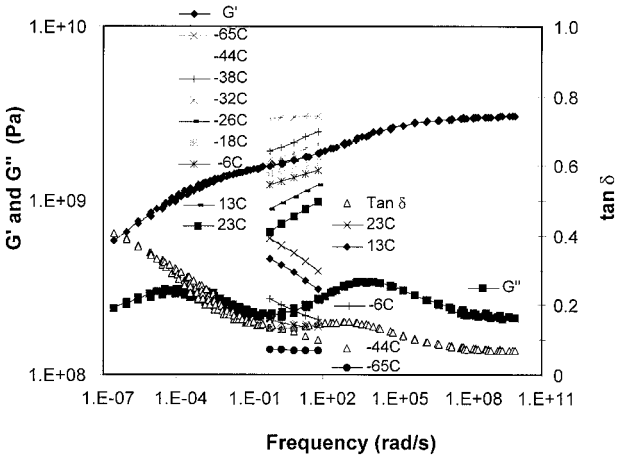

Figure 9 A master curve of PBX-9501 from data in Figure 8 was generated by shifting G', G'', and tan δ over the temperature range from −65 to 25°C.

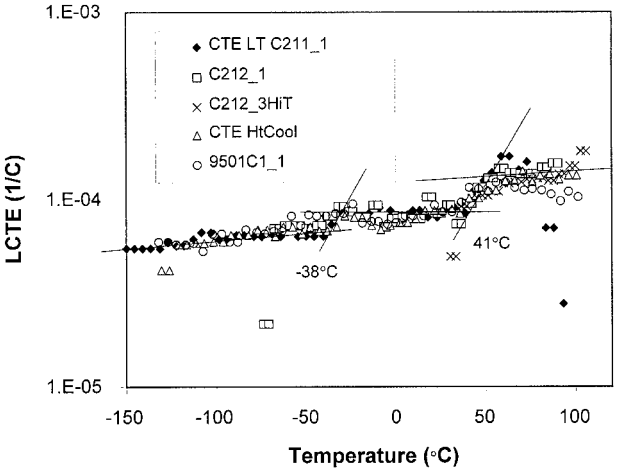

Figure 10 Linear coefficient of expansion measurements for LX-14 showed weak changes at approximately −35 and 41°C near the hard and soft segment loss tangent peaks.

Linear Coefficient of Expansion. The RMS 800 maintains a constant compressive load on the specimen under test. As the temperature is increased, the sample expands and the length of the fixture is adjusted to restore constant load. The change in length is recorded and a linear expansion coefficient (LCTE or α_1) is calculated according to

$$L_1 = L_0(1 + \alpha_1\Delta T) \quad \text{or} \quad \alpha_1 = (1/L_0)(\Delta L/\Delta T) \quad (9)$$

where L_0 is the original length and L_1 is the length after the change in temperature (ΔT). Above and below the glass transition, the coefficient of thermal expansion should increase continuously with temperature.[43] Figure 10 shows the result from 4 sets of LCTE measurements on LX-14 from −140 to 120°C. From about −150 to −40°C, below T_g(SS), the thermal expansion coefficient seems to follow a linear increase with temperature of the form

$$\alpha_1 = mT + \alpha_0 \quad (10)$$

Although the scatter is large for temperature T in degrees Celsius, the average value of the temperature dependence (slope) from about −120 to −38°C was 1.78 E-7 with the intercept at 0°C of $\alpha_0 = 7.91 \pm 0.4$ E-5. Over the range from −38 to −30°C there is a slight discontinuity in α_1 consistent with the soft segment glass transition (indicated in Fig. 10 by a line). The slope of the expan-

Table V Coefficients of the Temperature Dependence of Sub T_g(SS) Linear Coefficient of Thermal Expansion for LX-14 and PBX 9501 Fitted to Eq. (9)

Sample	Slope	α_0 (°C)	r^2	$\sigma(\alpha)$	T (°C)
LX-14_A1	1.782E-7	7.912E-5	0.8731	4.1E-6	−120 to −38
PBX-9501					
C3_1	1.518E-7	8.307E-5	0.806	4.4E-6	−120 to 0
C3_2	2.61E-7	8E-5	0.6504	8.2E-6	−120 to 0
PR1_2	2.214E-7	8.46E-5	0.9447	1.9E-6	−150 to −50
PR2_2	2.68E-7	7.13E-5	0.175	3.6e-6	−120 to 0
D2_2	1.50E-7	7.90E-5	0.840	2.2E-6	−150 to −50
D2_3	1.36E-7	9.05E-5	0.573	4.1E-6	−150 to −50
D3_1	1.53E-7	9.70E-5	0.666	3.9E-6	−150 to −50
E2_4	1.54E-7	8.67E-5	0.757	3.2E-6	−150 to −50
E2_6	1.522E-7	8.40E-5	0.763	3.0E-6	−150 to −50

sion coefficient increased slightly until between about 36 and 60°C a second discontinuity associated with the hard segment glass transition was observed. The midpoint of the discontinuity gave $T_g(\mathrm{SS})_\alpha$ of −34°C and $T_g(\mathrm{HS})_\alpha$ of 46°C. Above about 60°C the coefficient settles down again. Linear fits for various individual samples are given in Table V.

The thermal expansion of samples of PBX-9501 is not as clear-cut as LX-14. These samples were fairly linear up to about −50°C in several instances. Again the scatter is large and the average value of the temperature dependence (slope) from about −150 to −50°C was 1.53 E-7 for field return samples and 1.5–2.7 E-7 for control samples with the intercept at 0°C (α_0) of about 8.5 E-5.

Low Temperature Shear Storage Modulus. If the frequency dependence is neglected, the shear storage modulus (G') below T_g(SS) of LX-14 can be fitted to a simple linear temperature dependence of the form[44]:

$$\log G'_1 = K\Delta T + \log G'_0 \tag{11}$$

where K is the temperature coefficient of the low temperature shear storage modulus and G'_1 and G'_0 are shear storage moduli at T_1 and T_0. In Figure 4 the dotted line approximates the fit of eq. (11) to a single frequency data set of G' vs T values. The fit is reasonable up until the glass transition where the storage modulus drops off dramatically as the Estane binder passes through

Table VI Sub T_g Shear Storage Modulus Fits to Eqs. (10) Show Negative and Positive K Values for Different Runs of PBX-9501

Sample	K (Slope)	Intercept	G' (0°C) GPa	r^2
LX-14A	−6.192E-4	9.3384	2.18 ± 0.04	0.928
PBX-9501				
C3_1	−3.895E-4	9.4513	2.83 ± 0.05	0.852
C3_2	−1.120E-4	9.3827	2.41 ± 0.02	0.569
PR1_2	−4.339E-4	9.307	2.03 ± 0.02	0.896
PR2_2	5.503E-4	9.384	2.42 ± 0.02	0.326
D2_2	−5.502E-4	9.4571	2.86 ± 0.1	0.755
D2_3	−1.117E-4	9.4312	2.70 ± 0.04	0.410
D3_1	1.578E-4	9.3258	2.12 ± 0.05	0.645
E2_4	5.220E-4	9.2703	1.86 ± 0.03	0.902
E2_5	8.320E-4	8.9738	0.941 ± 0.04	0.983
E2_6	10.74E-4	8.6823	0.481 ± 0.006	0.982
E3_1	−7.694E-4	9.4267	2.67 ± 0.04	0.913

All frequency fits.

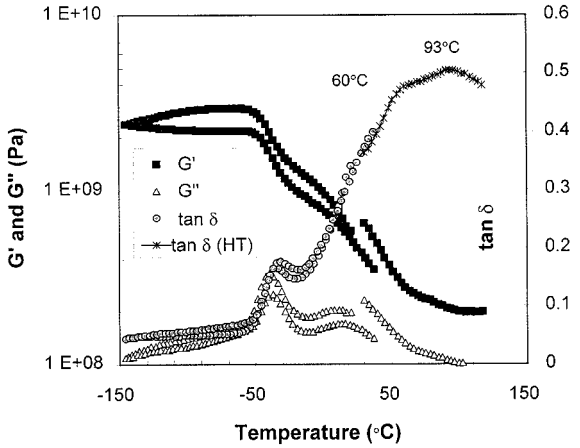

Figure 11 Higher moduli were found during cooling measurements than subsequent heating at identical rates in PBX-9501 (PR1_1,2,3).

its soft segment glass transition. Since there is no frequency dependence in eq. (11), the fits to all frequencies are not expected to be very good. The slope from −150 to −40°C was −6.19 E4 and G(0°C) was 2.18 E9 Pa for LX-14.

When different runs of PBX-9501 were fitted to eq. (11), different temperature coefficients were observed. Usually a negative temperature coefficient would be expected for the modulus below T_g(SS). However, in 5 cases the coefficient was positive, implying a reduction in modulus occurred as the PBX was cooled. To evaluate this, the samples were measured during cooling as well as heating. Figure 11 shows the dynamic mechanical moduli of PBX-9501 (sample PR1) during a cooling cycle followed by a heating cycle at about 1°C/min in both directions. A positive temperature coefficient was found during cooling and a negative temperature coefficient during heating. The shear storage and loss moduli were substantially larger during cooling than heating. The reason for this effect is not known. In PBX-9501 the moduli do not recover completely at T_g(SS), but are significantly different up to T_{eu}(NP) or about 20°C. The nitroplasticizer in PBX-9501 extended the temperature range over which the difference between moduli measured during cooling and heating was observed. The largest differences in G' for PBX-9501 on cooling compared to heating occurred between T_g(SS) and the lowest measured temperature and again between T_g(SS) and T_{eu}(NP). The shear storage modulus returns to nearly constant values at temperatures just below ambient but the loss modulus did not. When the sample is allowed to remain at ambient for one or two days then measured during heating from ambient, the moduli had shifted upward toward the cool down values as shown in Figure 11. Note that G' and G'' recovered to about the same extent because the tan δ traces (G''/G') overlap. This seems to imply that some type of recovery process is occurring, possibly resolubilization of the plasticizer in the Estane soft segment or changes in soft segment crystallinity. More experiments need to be performed to verify this.

Similar results were found for LX-14 (shown in Fig. 12) during cooling and heating measurements. In LX-14 the difference in modulus was most pronounced between −100 and T_g(SS). Above this temperature the moduli measured during cooling and heating tend to coalesce. Clearly, the presence of NP exacerbates the differences but is not solely responsible.

Effect of NP

In PBX-9501 there is a relaxation, T_{eu}(NP), just below ambient, between 4 and 16°C. This transition reflects a change in mobility of the binder/plasticizer near the NP eutectic temperature that occurs at about 12°C in the neat energetic plasticizer.[36] The plasticizer has a tendency to supercool and the maximum in the loss modulus at 1 Hz on cooling was consistently 5–8°C while the heating curve peaked between 8 to 16°C. No eutectic freezing or melting peaks were observed in the MDSC in Figure 3 of the 50/50 NP/Estane mixture, presumably because of this ability of NP

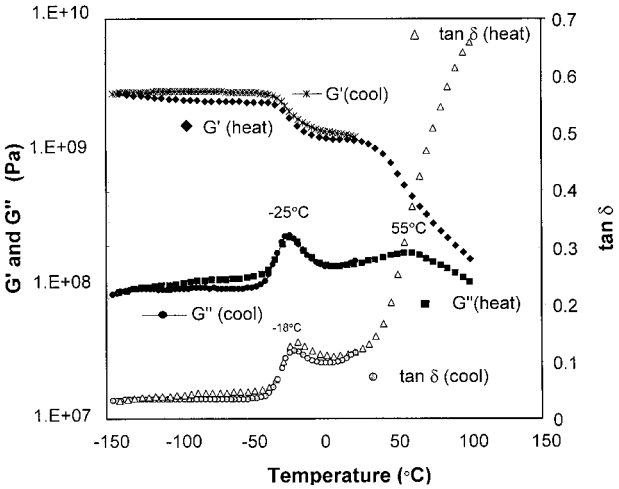

Figure 12 Cooling and heating dynamic mechanical measurements at identical rates showed less difference in both LX-14.

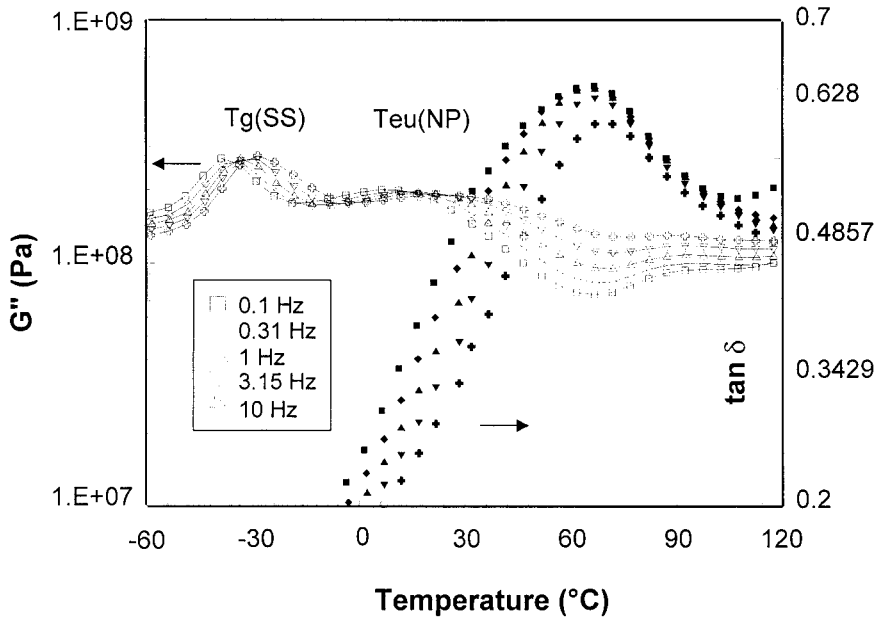

Figure 13 Comparison of PBX-9501 C3_2 spectra over 5 frequencies shows anamolous frequency dependence in the high temperature loss tangent peak.

to supercool. Once the soft segment has vitrified, NP can no longer crystallize and would be trapped by the high viscosity of the glassy soft segment. The kinetics of supercooling may help explain the difference in moduli in PBX-9501 during heating and cooling above T_g(SS). If volume changes occur due to crystallization of the NP, microvoids could form in the binder or at the HMX–binder interface, reducing the modulus. In the cooling and heating trace for PBX-9501 (in Fig. 11), there is recovery of the moduli overnight between the time the sample was run up to 40°C and rerun from 20 to 120°C. Again this seems consistent with redissolution of the NP in the soft segment.

This NP transition in PBX-9501 has more influence on the modulus than the binder hard segment glass transition. The shear storage modulus dropped from 1.4E9 Pa at −10°C to 3.5E8 Pa at 50°C, just below T_g(HS) for PBX-9501. This is a drop of about an order of magnitude in shear modulus. Figure 13 shows T_{eu}(NP) as peaks in the loss modulus on the second run of PBX-9501 control sample No. 3 over 5 frequencies. In G'' the peak temperature increased with measurement frequency. The peaks are weaker in the second run because more soft segment is available to solubilize the NP. The frequency traces do not come together after the peak apparently because there is some Estane soft segment crystallinity. The characteristic frequency dependence of this mechanical relaxation suggests that it is associated with plasticizer mobility more than the actual phase separation of NP.

Ambient Behavior and Above

At least two different kinds of relaxations were expected above ambient in the dynamic mechanical spectra of Estane 5703p and the PBXs made from it. There should be a broad, slow reduction in modulus associated with the broad melting of soft segment crystals, consistent with the endotherm observed in the MDSC traces in Figures 2 and 3. In the first run, at least, there should also be some evidence of hard segment reinforcement. Although MDI-BDO hard segment melting has been observed between 200 and 250°C in urethanes with high hard segment content, MDSC measurements on Estane 5703 up to 250°C showed no clear evidence of a melting endotherm.

Vitrification of Estane 5703 Hard Segments

The hard segments of Estane 5703 are short chains of methylenebis(diphenylisocyanate) or MDI and butanediol.[1,2,11] The hard segment microphase is embedded in a matrix of soft segment polyester. Because these hard segments are attached to the soft segment matrix in blocks, they

are constrained, require some finite time to phase separate, and may perfect their structure over a very long time.[29,30] It is, therefore, not surprising that first and second runs of these explosives through temperatures above the hard segment glass transition will not yield identical dynamic mechanical spectra. This can be seen for LX-14 in Figure 4 where a second high temperature run is overlaid on the first run. The breadth and maxima in the loss modulus and tangent δ peaks changed as did the storage modulus. The peak in the loss modulus varied between 58 and 70°C. Note that the loss modulus peak occurred at somewhat lower temperature than its counterpart in Estane (~80°C) shown in Figure 1, but the maxima in tan δ was above 120°C in LX-14 and only 90°C in the binder. An increase in the breadth of the transition is characteristic of composite materials compared to the neat binder. Unfortunately, the effect of soft segment crystallinity and the hard segment glass transition could not be differentiated in LX-14.

The T_g(HS) in PBX-9501 is assumed to be associated with the maximum in the tan delta trace of first run measurements at about 71°C (see Fig. 5). The hard segment glass transition occurred at 66°C in the first MDSC scan of 50/50 binder/NP blends, but was not observed in second scans (see Fig. 3). In all first scans of PBX-9501 there was a peak at or above 70°C and a shoulder between 50 and 60°C. In the MDSC there was an endothermic peak at 49°C in plasticized Estane and at 53°C in pure Estane. This is slightly lower than the melting point of pure poly(butylene adipate).[25] The shoulder observed in first runs is believed to be due to melting of soft segment crystals. In dynamic mechanical measurements on PBX-9501 that had already been heated to 120°C, only a single peak was observed at between 65 and 66°C (see Fig. 13). This temperature is higher than the shoulder in first runs, implying slight improvement in crystallinity when the hard segments have not had sufficient time to reassociate. This is consistent with increased area under MDSC traces in the second run. The shape of the frequency curves in second scans above the peak show almost no shift, which is consistent with melting behavior.

Comparison of control sample C3 first and second runs in Figure 14 showed a reduction in storage modulus of about 15–23% in the second run from the initial low temperature value to the T_g(SS). This is similar to what was observed in heating and cooling behavior discussed previ-

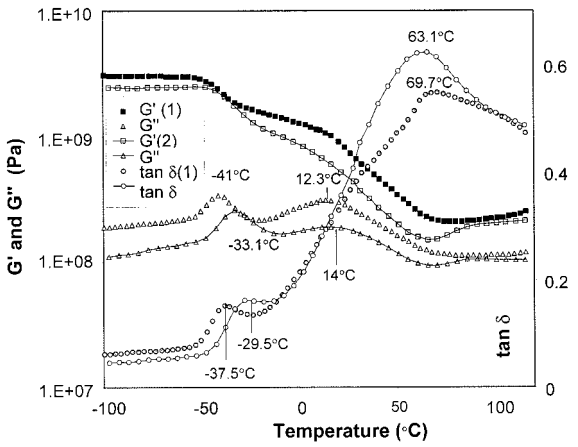

Figure 14 PBX-9501 control sample first and second runs showed changes in hard and soft segment transitions and NP associated with kinetic phenomena in binder and plasticizer.

ously. In the second run the soft segment glass transition is higher, indicating phase mixing of hard and soft segments. This result is at variance with the constant soft segment glass transition found in the MDSC for plasticized binder. In the second run the eutectic peak in G'' is less pronounced, also consistent with phase mixing. As discussed above second runs show only one broad relaxation in tan δ that peaks between 62 and 67°C due to soft segment melting. From above −30 to 70°C the shear storage modulus is consistently lower for the second run. Above about 75°C, the loss and storage moduli for first and second runs are similar, indicating that hard segment reinforcement and physical crosslinking responsible for the higher stiffness in first runs has been effectively removed. Based on elemental analysis of Estane 5703, the maximum hard segment content would be 30%. This is reduced by half in the Estane/NP formulations. It is surprising that there is any contribution from the Estane hard segments at all in the plasticized formulation. Two factors may help explain this weak contribution. First, the reduced solubility of the hard segment in NP would tend to enhance phase separation. Second, it has been shown in model compounds[45] that even low concentrations of hard segments will phase separate when the solubility parameters are sufficiently different.

Aged LX-14 and PBX-9501

A set of dynamic mechanical measurements were made on an experimental version of LX-14 that

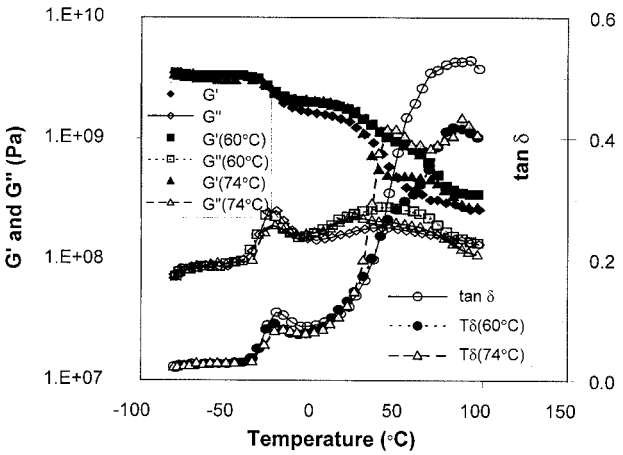

Figure 15 LX-14 samples aged in air for 3.75 years at ambient, 60, and 74°C showed the effect of chain scission on the dynamic mechanical properties.

had been aged for $3\frac{3}{4}$ years at ambient, 60 and 74°C. Figure 15, adapted from ref. 2, shows dynamic mechanical measurements from each aging temperature. As discussed in the reference, ester hydrolysis resulted in chain scission in the polyester soft segment. As the chains in the poly(ester urethane) undergo scission, the linkages between the hard and soft segments are reduced. This allows increased soft segment crystallinity as well as hard segment phase separation. In the ambient aged sample a very broad relaxation peak in tan δ (from 70 to 94°C) encompassed both soft segment melting and hard segment glass transition. Crystallinity is inhibited by the connectivity of the hard segments, reducing the stiffness (storage modulus) above the soft segment glass transition. As the number of chain scissions increased in samples aged at 60°C, increased soft segment crystallinity and hard segment perfection stiffened the binder (see 60°C traces) and a shoulder developed in the tan δ trace at 48.5°C. Substantial connectivity of the hard segment is still present in this aged sample since its storage modulus remains high above the melting point of the soft segments until the hard segment glass transition is exceeded at 85–90°C. As more degradation occurred, in the 74°C aged specimen, the crystalline soft segment shoulder in tan delta becomes a well-defined peak. Much lower connectivity between hard and soft segments caused the dramatic drop in storage modulus as the soft segment melted in LX-14 aged at 74°C.

By comparison to oven-aged LX-14, the degradation in field returned PBX-9501 was very benign. Both LLNL and LANL weapons were normally backfilled with dry, inert gas. As a result, degradation by ester hydrolysis, which is catalyzed by moisture,[5–7] was dramatically reduced. Dynamic mechanical spectra from each of the field return samples of PBX-9501 and the control sample were quite similar (see Fig. 16). Evidence of extensive chain scission was not observed in the field return samples of PBX-9501. It is known that NP can migrate out of PBX-9501. This being the case, there should be an increase in T_g(SS) as the NP is lost. Figure 16 shows at most an increase of 1.5°C in T_g(SS) for the oldest PBX-9501 consistent with small losses of plasticizer. However, this result is not definitive since minimal effort was made to prevent NP from migrating after the explosive was machined. Furthermore, a second sample of PBX-9501 from the 11-year-old material showed slightly lower T_g(SS). The shear storage moduli of field returns and control PBX-9501 are very nearly identical up to about 75°C. At about 50°C the oldest sample (D2_2) began to deviate from the others. At the end of the run, this sample had fractured completely. The crack probably started where the modulus began to fall. A second sample of the 11-year-old PBX-9501 that did not crack, D3_1, was very similar to the E2_2 and the control sample.

The only evidence that any ester hydrolysis occurred at all in the field return samples of PBX-9501 comes from the reduction in the rubbery plateau modulus above the hard segment glass transition with time in the field. In Figure 16 the

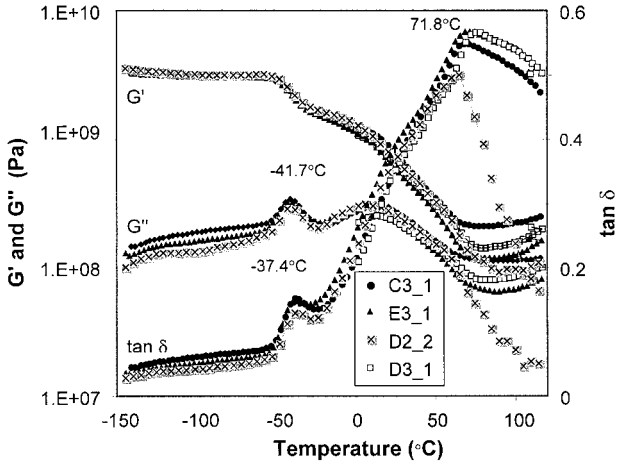

Figure 16 First runs of PBX-9501 from control (C3_1), 5.75-year (E3_1), and 11-year (D2_2 and D3_1) field-aged samples showed only small changes in T_g(SS) possibly associated with loss of NP during aging.

shear storage modulus above 70°C was greatest for the control sample and lower for the field-aged samples (E and D3_1). This is consistent with slight reduction in molecular weight between physical crosslinks (hard segments) in the binder. Another interesting observation was the development of a shoulder at about 90–95°C in tan δ. This shoulder occurred at approximately the same temperature as that observed in aged LX-14 hard segment peak, and could indicate that hydrolysis or another aging mechanism allows hard segments to further aggregate.

CONCLUSIONS

The hard and soft segment transitions for Estane 5703p could also been observed in two plastic bonded explosives which use this poly(ester urethane) as a binder even at concentrations as low as 2.5%. The soft segment transition in LX-14 explosive was 2°–3° higher than in the pure polymer, not because of antiplasticization by the explosive filler, but because low molecular weight oligomer was lost in the formulation process. In PBX 9501 the Estane 5703p soft segment was plasticized by the presence of NP, causing T_g(SS) to decrease by 15° compared to the pure polymer. The hard segment glass transition in Estane 5703p and the 2 PBXs is only observed in the first measurement. This is consistent with indications from the literature that some time is required for reassociation of these hard segments once they have been redissolved in the soft segment.

Crystallinity in the soft segment is observed as a low temperature shoulder in Estane and the PBXs. This shoulder became a peak in second and subsequent runs at about 60–65°C in PBX-9501. When aged in humid atmosphere, this shoulder can develop into a peak in LX-14 depending on the extent of ester hydrolysis.

In PBX-9501 a new polymer–plasticizer peak was observed near the eutectic melting point of NP. Cooling measurements showed this transition at lower temperatures than heating measurements. Moduli measured during cooling from ambient were greater than those measured during heating in both LX-14 and PBX-9501. The plasticizer enhanced the magnitude of this difference in modulus and the range over which it occurred. Aged PBX-9501 from field returns may show slight loss of plasticizer with time but not enough to definitively change T_g(SS).

Because very little catalytic moisture is available in weapons, ester hydrolysis from field aged PBX-9501 was much lower than oven-aged LX-14. Increases in T_g(HS) and reduction in plateau modulus at elevated temperatures indicate mild aging in PBX-9501.

Randy Weese provided the MDSC data. Jim LeMay and Greg Buntain supplied some of the PBX-9501 samples. Funding for this effort was provided in part by the Dual Revalidation Program under the direction of Cynthia Nitta, Keith Bradley, and Roger Logan, and is gratefully acknowledged.

REFERENCES

1. Grotheer, E. W. BDX-613-3849; Allied Signal Bendix Kansas City Division: Kansas City, MO, January 1988.
2. Hoffman, D. M.; Caley, L. E. Org Coat Appl Polym Sci Proc 1981, 44, 686.
3. Flowers, G. L. MHSMP-85-42; Mason and Hanger Co., Pantex Plant: Amarillo, TX, August 1985.
4. Baker, G. K. BKC-18-926-3698; Allied Signal Corporation Kansas City Division: Kansas City, MO, Aug. 6, 1975.
5. Brown, D. W.; Lowry, R. E.; Smith, L. E. Macromolecules 1980, 13, 248.
6. Brown, D. W.; Lowry, R. E.; Smith, L. E. Macromolecules 1981, 14, 65.
7. Brown, D. W.; Lowry, R. E.; Smith, L. E. Macromolecules 1982, 15, 453.
8. Faubion, B. D. MHSMP-86-24; Mason and Hanger Co., Pantex Plant: Amarillo, TX, 1986.
9. Rabie, R. L. LA-CP-95-117; Los Alamos National Laboratory, Los Alamos National Laboratory: Los Alamos, NM, May 1995.

10. Pack, R. T. LA-UR-98-6014; Los Alamos National Laboratory: Los Alamos, NM, 1998.
11. Overturf, G. E., III; LeMay, J. D.; Russell, B.; Nonidez, W.; Mays, J.; Haining, H. J.; Kober, E. M. UCRL-JC-133769; Lawrence Livermore National Laboratory: Livermore, CA, March 1999.
12. Humphrey, J. R. UCRL 52350; Lawrence Livermore National Laboratory: Livermore, CA, November 1977.
13. Skidmore, C. B.; Phillips, D. S.; Son, S. F.; Asay, B. W. LA-UR-97-2596; Los Alamos National Laboratory: Los Alamos, NM, March 1997.
14. Skidmore, C. B.; Phillips, D. S.; Crane, N. B. LA-UR-97-2807; Los Alamos National Laboratory: Los Alamos, NM, 1997.
15. Kasprzyk, D. J.; Bell, D. A.; Flesner, R. L.; Larson, S. A. Prop, Explosives Pyrotech, 1999, 24, 333.
16. Browning, R.; Meyer, T. Presented at the JOWOG Workshop, Lawrence Livermore National Laboratory, Livermore, CA, August 1999.
17. Shaw, M. T.; Price, J. R.; Hoddinott, M. J Rheol 1979, 23, 403.
18. Hamstad, M. A. TID-4500, UC-25; Lawrence Livermore National Laboratory: Livermore, CA, October 24, 1967.
19. Hoffman, D. M. J Energ Mat 2001, 19, 163.
20. Townend, D. J.; Warren, R. C. Polymer 1985, 26, 79.
21. Estes, G. M.; Cooper, S. L.; Tobolsky, V. A. J Macromol Sci-Rev Macromol Chem 1970, C4, 167.
22. Petrovic, Z. S.; Ferguson, J. Prog Polym Sci 1991, 15, 695.
23. Hepburn, C. Polyurethane Elastomers; Applied Science Publishers: London, 1973.
24. MacKnight, W. J.; Yang, M.; Kajiyama, T. Polym Prepr (ACS, Div Polym Chem) 1968, 9, 860.
25. Zilberman, E. N.; Kulikova, A. E.; Teplyakov, N. M. J Polym Sci 1962, 56, 417.
26. Leung, L. M.; Koberstein, J. T. Macromolecules 1986, 19, 706.
27. Camberlin, Y.; Pascault, J. P. J Polym Sci, Polym Chem Ed 1983, 21, 415.
28. Hesketh, T. R.; van Bogart, J. W. C.; Cooper, L. L. Polym Eng Sci 1980, 20, 190.
29. Musselman, G. S.; Santosusso, T. M.; Barnes, J. D.; Sperling, L. H. J Polym Sci, Polym Phys Ed 1999, 37, 2586.
30. Orler, E. B. Unpublished results; Los Alamos National Laboratory, Los Alamos, NM, 1999.
31. Kwei, T. K. J Appl Polym Sci 1982, 27, 2891.
32. Chee, K. K.; Farris, R. J. J Appl Polym Sci 1984, 29, 2529.
33. Aitken, R. R.; Jeffs, G. M. F. Polymer 1977, 18, 197.
34. Yen, M. S.; Cheng, K. L. J Appl Polym Sci 1994, 52, 1707.
35. Privalko, V. P.; Privalko, E. G.; Shtompel, V. I.; Pissis, P.; Kanapitsas, A.; Pradas, M. M.; Ribelles, J.-L. G. Polym Eng Sci 1999, 39, 1534.
36. Shen, S.-M.; Leu, A.-L.; Chen, S.-I.; Yeh, H.-C. Thermochem Acta 1991, 180, 251.
37. Fox, T. G. Bull Am Phys Soc 1956, 1, 123.
38. Rivera, T. LA-5313; Los Alamos National Laboratory: Los Alamos, NM, May 1973.
39. Mang, J. T.; Skidmore, C. B.; Hjelm, R. P.; Howe, P. M.; Rieker, T. P. Presented at JOWOG-9, Lawrence Livermore National Laboratory, Livermore, CA, August 1999.
40. Song, Y. M.; Chen, W. C.; Yu, T. L.; Linliu, K.; Tseng, Y. H. J Appl Polym Sci 1996, 62, 827.
41. Ferry, J. D. Viscoelastic Properties of Polymers; John Wiley & Sons: New York, 1980; Chap 11.
42. McCrum, N. G.; Read, B. E.; Williams, G. Anaelastic and Dielectric Effects in Polymeric Solids; John Wiley & Sons: New York, 1967.
43. Allcock, H. R.; Lampe, F. W. Contemporary Polymer Chemistry; Prentice-Hall, 1981; 434–435.
44. Bechwith, T. G.; Buck, N. L.; Marangoni, R. D. Mechanical Measurements; Addison-Wesley: Reading, MA, 1982; pp 114–119.
45. Tonelli, C.; Bassi, M.; Ajroldi, G. J Polym Sci Part B Polym Phys 1999, 37, 1609.